A new human-like walking for the humanoid robot Romeo

A Kalouguine, V De-León-Gómez, C Chevallereau, S Dalibard, Yannick Aoustin

Noname manuscript No.
(will be inserted by the editor)

A new human-like walking for the humanoid robot *Romeo*.

A. Kalouguine[1,2], V. De-León-Gómez[3], C. Chevallereau[1], S. Dalibard[2], Y. Aoustin[1*]
[1] **Laboratoire des Sciences du Numérique de Nantes,**
CNRS UMR6004, Université de Nantes,
France,
[*] **Corresponding author**
[2] **SoftBank Robotics,**
43, Rue du Colonel Pierre Avia 75015 Paris,
France.
[3] **Universidad Autónoma de Coahuila,**
Blvr. Revolución, 151 ote. Torreón, México

April 12, 2022

Abstract

This paper seeks to define the anthropomorphic walking motion for the humanoid robot *Romeo*. The main characteristics of the lower and upper limb motions of the human being during walking are adapted to *Romeo* taking into account its kinematics and its motor power. The proposed walking includes starting, periodic and stopping motions. A boundary value problem is stated and solved to define each of these three movements, which are composed of single and double support phases. The trajectory of the zero moment point (ZMP) is explicitly defined as a function of time. Thanks to the *Essential model*, the two horizontal coordinates of the center of mass (CoM) are adapted to the desired ZMP trajectory and joint movements of *Romeo*. Numerical results show the efficiency of our strategy to design human-like walking for *Romeo*.

Keywords: Human-like walking, *Essential model*, Starting motion, Stopping motion, Periodic Motion, Boundary value problem.

1 Introduction

A humanoid robot that is programmed to walk like a human initiates a certain interest and a level of affinity in people [1]. This feature is important to improve the acceptability to humans of a humanoid robot that interacts with them to perform common tasks. Human-like walking for a humanoid robot is currently a challenging paradigm for the robotics community. However, due to the different characteristics between human and humanoid robot (mass distribution, number of joints, actuation, etc), the choice of walking gait and control approaches are generally based on models of humanoid robot.

One proposal is to use parametric optimization, which can be an efficient tool to design a human-like walking for a humanoid robot, [2]. However, walking composed of simple support phases and impacts remains very rudimentary. Besides, the high cost in computing time trajectories makes it difficult to adapt the humanoid robot's speed online. Another obstacle is the limited number of degrees of freedom (DoF) of a humanoid robot compared to a human whose joints are complex and almost frictionless. Moreover, the weight-to-power ratio of humanoid robots with rigid bodies is not as high as it would need to be to allow human-like walking. Let us remark however, an interesting work of Ames [3] who proposes to define articular variables for *Nao*, whose behavior is described by a time solution of a linear mass-spring-damper system. The parameters of this function are directly taken from human gait data. To overcome the mechanical complexity of humanoid robots and efficiently implement walking algorithms, Kajita *et al* [4] proposes the linear inverted pendulum model (LIP). The humanoid robot is represented by its CoM, which concentrates the overall mass of the robot and is connected to the ZMP by a massless leg. The altitude of the CoM is assumed constant. The dynamic model of the pendulum is therefore linear. Razavi *et al* [5] proved that a 3D LIP, which is a symmetric hybrid system (SHS) can have an infinite number of synchronized periodic orbits that can be neutrally stable in kinetic energy. Koolen *et al* [6] proves that the introduction of the instantaneous capture point ICP allows to reduce the complexity of the control by applying it only to the relation between the ZMP and the ICP, the relation between the ICP and the CoM is left free since it has a naturally stable dynamics. The ICP is also an efficient tool to produce stopping motion. A drawback of the LIP model is to generate walking trajectories in which the knees must always be bent in order to avoid any problem of geometric singularity in the lower limbs. Moreover, the assumption of a linear motion of the estimated CoM of the whole body is not verified in recorded data of human walking, where a vertical oscillation of the CoM is observed, see for example [7] or [8]. Furthermore it is shown in [9] that conditions for self-synchronization and vertical displacement of the CoM lead to stable gaits of a 3D biped. About the upper limbs several works prove that the dynamic effects of the arms cannot be neglected. For example Collins *et al* [10] show simulation results and experimental data supporting the hypothesis that the primary function of arms swinging during gait is to reduce the fluctuations of the vertical angular momentum with respect to the CoM of the body due to external moment requirements or perturbations. Aoustin and Formal'skii [11] proved that for a given time period and a given length of the walking gait step, there is an optimal swinging magnitude of the arms with respect to an energy cost. It is therefore difficult to deal with the trade-off between a simple linear model such as LIP and the design of a human-like walking.

The purpose of this paper is to analyze the main characteristics of human gait in order to adapt them to design a gait for the humanoid *Romeo*, which has 31 DoF, taking into account its technological limits. A common approach is to define polynomial functions parameterized with human motion data and to run them on the humanoid robot. However, most of the cases, this strategy leads to a problem of instability of the humanoid robot's walk. Indeed in this case the ZMP usually comes out of the support polygon. To overcome this difficulty, one possibility is to modified the human motion to satisfy the equilibrium condition as it is done in imitation techniques for static [12] or dynamic motion [13, 14]. We choose another solution, the ZMP trajectory could be imposed instead of the CoM. To carry out this choice, a strategy based on the *Essential model* [15] is developed. The placement of the ZMP is imposed at all times.

The temporal evolution of reference points on several body parts (such as the torso, arms, feet) is defined so as to impose 29 DoF. Two DoF, the horizontal components of the CoM are left free in order to allow for the chosen placement of the ZMP. The interest of using the *Essential model* is to ensure dynamic equilibrium for any walk, which would be very difficult to achieve without this tool. In this companion article to [15], our main contribution is to use this tool and be inspired by the characteristic movements of the human upper and lower limbs to design a complete and dynamically stable walk for a humanoid robot. This complete humanoid walking is designed, with a starting phase, a periodic walk, and a stopping phase. Each of these three phases is found by solving a boundary value problem, which defines a fluent bio-inspired CoM trajectory of the robot. Unlike other papers [3, 16], the stability is insured by the proposed methodology. The interaction with the ground is a sequence of foot flat contacts in single and double support phases.

The paper is outlined as follows. Several characteristics of human walking are recalled in section 2. These characteristics are adapted to design a human-like walking in section 3. Section 4 presents the *Essential model*, which is used to calculate the CoM trajectory corresponding to a prescribed ZMP trajectory. The definition of the periodic walking motion and the boundary value problem used to find it are described in section 5. Section 6 presents solutions for the starting and stopping phase problems. Numerical results are gathered in section 7. Section 8 offers the conclusion and perspectives.

2 Main characteristics of human walking.

The main characteristics of a human gait are recalled, since the goal is to make the most human-like walking possible for *Romeo*.

Duration of different phases: Human gait can be decomposed according to important events that occur during the walking. A gait cycle consists of two steps. The durations T_{SS} of the single support (SS) phase and T_{DS} of the double support (DS) phase are measured as a percentage of a cycle period. These durations T_{SS} and T_{DS} depend on the walking speed. The percentage of the double support phase varies from 9 to 17% depending on the age and velocity of the human [17]. The faster the human walks, the shorter the walking period $T = T_{SS} + T_{DS}$ and the lower the proportion $\frac{T_{DS}}{T_{DS}+T_{SS}}$. A typical distribution of walking at a comfortable speed is presented in Fig. 1.

Step placement: The step length and width vary widely depending on morphology and age. For a young healthy adult the step length varies widely (from 0.40 to 0.80 m for larger velocities), same as the step width (from 0.125 to 0.22 m, with width decreasing for larger velocities) [17, 18].

CoM Trajectory: Human CoM trajectory is close to a sinusoidal function in longitudinal, transverse and vertical directions [17]. The magnitude and period of oscillations in transverse direction vary with speed [19]. In vertical direction, the magnitude of the displacement increases with velocity and is equal to about 2% of body height.

ZMP trajectory: The ZMP goes from the heel to the tip of each foot [20], which corresponds to the rolling motion of the feet and the mobility of the human sole, see Fig. 2. The trajectory of the ZMP changes depending on the footwear of the human [21].

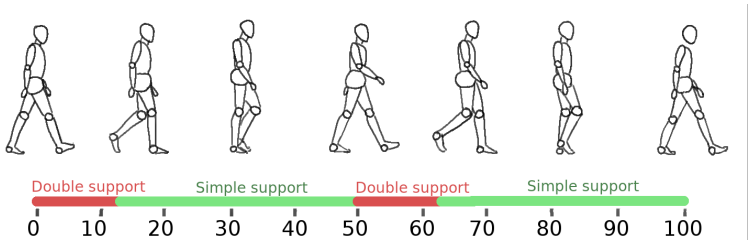

Fig. 1: SS and DS phase durations, measured as percentage of complete cycle.

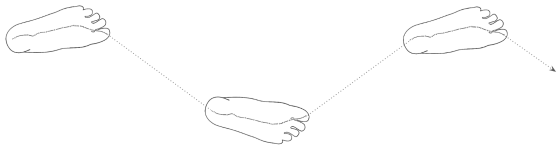

Fig. 2: Periodic human walking: illustration of a ZMP trajectory, inspired from [20].

Swing foot motion: The motion of the swing foot can be separated into two components, the trajectory of one point of the foot and the orientation of the sole. We observe nearly vertical landing and take off trajectories, with most of the horizontal movement performed in the middle of the SS.

Trunk motion: The trunk, which represents 60% of the weight, has significant angular oscillations [22]: in the sagittal plane, the magnitude is about 2° around the equilibrium position (which varies with the walking velocity but is typically between 5 and 13°, leaning forward). In the frontal plane, the oscillation magnitude varies from 3° to 6° from large to small velocities respectively.

Hip motion: The rotation of the pelvis around the vertical axis allows for larger steps, and helps to smooth out the trajectory of the CoM. The magnitude of the oscillations around the vertical axis is of about 10° [17].

Arm swing: The arm swing in human locomotion is speculated to be useful to reduce the contact wrench on the support foot, as well as the global cost of walking [23], [24].

3 Human trajectory and humanoid robot

Most humanoid robots are close to human in their proportions. However the number of DoF is lower than that of the humans, body parts are rigid, and their motor power is very limited with respect to their weight. Moreover, the motion of the human locomotor system is hard to reproduce exactly, as it is a complex system with passive and active nonlinear actuations. Therefore, an adaptation of these characteristics of the human walk characteristics is necessary to define an anthropomorphic gait for a humanoid robot. In this section biomechanical characteristics of human walking are used to define a walking movement suitable for our humanoid robot *Romeo*. Despite this adaptation, numerical tests show that this approach does not allow to obtain a viable walking motion with the considered humanoid *Romeo*.

3.1 Humanoid robot *Romeo*

The humanoid robot considered in this study is *Romeo*, a humanoid platform developed by the company Softbank Robotics, see Fig. 3 a). It is 1.47 m tall and weighs 36 kg. *Romeo* features 31 revolute joints, which are distributed such as: for each leg two at the ankle, one at the knee, and three at the hip; for each arm three at the wrist, two at the elbow, and two at the shoulder; one for the torso; four for the neck and head. The 31 joint variables are gathered into the into the joint vector $q \in \mathbb{R}^{31\times 1}$. The body parts of *Romeo* are mostly rigid.

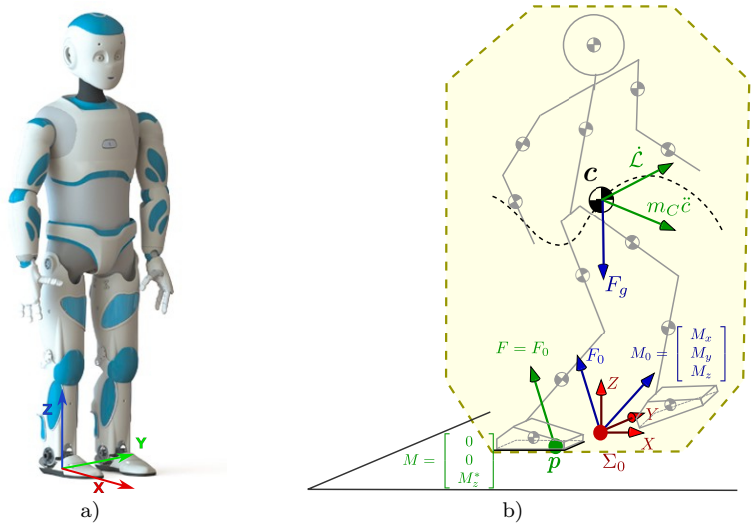

a) b)

Fig. 3: a) Photography of *Romeo*. b) Illustration of the global equilibrium.

3.2 Adaptation of the parameters of human trajectories to *Romeo*

The duration T_{DS} of the DS phases is chosen to be 10% (close to 12%, value that has been observed for the human walk [17]) of the cycle duration $2T$, where $T = T_{DS}+T_{SS}$, with $T_{DS} = 0.15$ s and $T_{SS} = 0.60$ s. For current humanoid robots [4, 25], it is impossible to achieve a step size of 0.75 m as what is observed for humans, because the rolling motion of the stance foot is necessary for these larger steps, see [26, 27]. Therefore, it is necessary to adapt the parameters of trajectories for *Romeo*. The step length is chosen within the range 0.15 to 0.20 m, which corresponds to a 0.30-0.40 m displacement of the swing foot with a velocity of 0.83 to 1.1 km/h. The step width is chosen to be 0.20 m, satisfying a safe clearance between *Romeo*'s ankles. The objective is to design a non-impact walk at the end of the SS phase. The speed of the swing foot is therefore imposed to be zero when it touches the ground. During the SS phase, a quadratic-cycloidal B-splines [15] is used to define the trajectory of the swing foot.

A summary of the other adaptations is shown in Table 1. Most periodic functions are approximated by a sinusoidal function to have a simple model that is infinitely differentiable. Once the human walking motion has been adapted to the $n = 31$ variables

Table 1: Main parameters of the trajectories for *Romeo*

Variable	Period	Mean Value	Magnitude	Feature
Motion along Z-axis of the CoM	T	1.12×(leg length)	about 2% of height	Minimum in middle of DS
Motion along X-axis of the CoM	linear progression	–	–	–
Motion along Y-axis of the CoM	T	0 m	Same as Z-axis	Zero around 80% of DS
Trunk roll	T	0°	5°	Minimum in middle of DS
Trunk pitch	T	6°	2°	Maximum at beginning and end of DS
Trunk yaw	$2T$	0°	5°	Maximum at beginning of swing phase
Swing foot Height	Zero in DS Cycloid in SS	–	0.02 m	Maximum in middle of SS
Swing foot Pitch	Zero in DS Cycloid in SS	–	−20° to 81°	Minimum right after impact.
Shoulder pitch	T	7.5 ∘	0° to 25°	
Elbow pitch	T	32.5 ∘	0° to 25°	

of *Romeo*, it can be tested on the robot model. Due to the humanoid robot dynamics, the ZMP trajectory $(p_x, p_y, 0)$ resulting from the human gait parameters, may not satisfy the equilibrium condition.

Therefore, in order to avoid this problem and ensure dynamic equilibrium, one possible solution is to impose the ZMP trajectory instead of the CoM. Thus, to carry out this objective, a strategy based on the *Essential model* is proposed in the next section.

4 Essential model

The *Essential model* is first introduced in [15]. The purpose of the *Essential model* of a humanoid robot (*i. e.* here *Romeo*) is, from the desired trajectory of its ZMP, the desired orientation of its trunk, the desired position and orientation of its swing foot, the desired articular variables of the upper body, to compute the horizontal behavior of its CoM. The essential model thus makes possible to take into account the global behavior of the robot, as opposite to models based on the inverted pendulum. The joint variables induced (geometrically and dynamically) by this model have to be compatible with the following characteristics of its actuators, like maximum torques. A hypothesis of perfect control tracking is adopted in the calculation of ground reaction forces, position of the ZMP and the torques resulting from these trajectories.
In this study, the designed walking motion has to satisfy the following conditions:

1. Walking must be visually anthropomorphic,
2. The global ZMP of the robot must at all times be within the support area,
3. The interaction with the ground must be a sequence of foot flat contacts imposed in single and double support phases.

The first and third conditions depend on the designed trajectories and capabilities of the robot. The second condition is satisfied, since the placement $(p_x, p_y, 0)$ of the ZMP is imposed at each time thanks to the essential model. However, in order to do this, it is necessary to let two coordinates free or not directly controlled. The x and y coordinates of the CoM are chosen as free. This section presents the development stages of the *Essential model* for *Romeo*.

4.1 Centroidal model

The Centroidal dynamics are frequently used in robotic walking, especially for humanoid robots [28] [29]. The centroidal model considers the dynamics of the humanoid robot around its CoM. It allows the acceleration of the CoM to be expressed as a function of the external forces acting on the humanoid robot, and thus, to define the position $(p_x,\ p_y)$ of the ZMP on the ground as follows:

$$\begin{aligned} m\ddot{X} &= \sum_{k=1}^{N} F_k + mg \\ \dot{\mathcal{L}} &= \sum_{k=1}^{N} (p_k - X) \times F_k + \sum_{k=1}^{N} M_k \end{aligned} \tag{1}$$

where:

- N is the number of contacts with the environment,
- $X = (x, y, z)^\top \in \mathbb{R}^3$ is the position vector of the CoM,
- $F_k \in \mathbb{R}^3$ is the net force exerted by the k^{th} contact,
- $M_k \in \mathbb{R}^3$ is the moment exerted by the k^{th} contact,
- m (kg) is the global mass of the robot,
- $g = 9.81$ (m/s^2), is the gravity constant,
- $\mathcal{L}$ is the angular momentum calculated in the CoM of the humanoid robot,
- $p_k \in \mathbb{R}^3$ is the point of application of the net force of the k^{th} contact. If the contact is not punctual, p_k is the center of pressure (CoP).

In a normal gait, the external efforts acting on a humanoid robot are the gravity force $\boldsymbol{F}_g$ and the ground reaction efforts acting at each foot, as shown in Fig. 3 b). The resultant effort caused by the ground reaction is defined by the wrench $(\boldsymbol{F}_0, \boldsymbol{M}_p)^\top = (F_x, F_y, F_z, 0, 0, M_z^*)^\top$ and is applied at the global ZMP, denoted as $\boldsymbol{p} = (p_x, p_y, 0)^\top$. The model (1) defining the global equilibrium at the CoM of the humanoid robot becomes:

$$\begin{aligned} p_x &= x - \frac{z\ddot{x}}{\ddot{z} + g} - \frac{\dot{\mathcal{L}}_y}{m(\ddot{z} + g)}, \\ p_y &= y - \frac{z\ddot{y}}{\ddot{z} + g} + \frac{\dot{\mathcal{L}}_x}{m(\ddot{z} + g)}. \end{aligned} \tag{2}$$

The position of $\boldsymbol{p}$ can be calculated with the following equation of moment equilibrium at the world frame Σ_0:

$$\boldsymbol{M}_0 = \boldsymbol{p} \times \boldsymbol{F}_0 + \boldsymbol{M}_p, \tag{3}$$

where $\boldsymbol{M}_0^\top = (M_x, M_y, M_z)^\top$. The horizontal coordinates of the ZMP p_x and p_y can be expressed from (3) as follows:

$$\begin{aligned} p_x F_z + M_x &= 0 \\ p_y F_z - M_y &= 0 \end{aligned} \tag{4}$$

The ZMP $\boldsymbol{p} = (p_x, p_y, 0)^\top$ must be inside the convex hull of support for all time in order to satisfy the dynamic equilibrium condition of the humanoid robot [30].

In DS the global ZMP is the barycenter of the two local ZMP p_1 and p_2, one in each foot. The efforts of the ground reaction produce the global wrench $(\boldsymbol{F}_0, \boldsymbol{M}_0)^\top$ in p, which can be divided on the wrenches $(\boldsymbol{F}_1, \boldsymbol{M}_{p1})^\top$ in p_1 and $(\boldsymbol{F}_2, \boldsymbol{M}_{p2})^\top$ in p_2, such as:

$$\begin{aligned} F_0 &= F_1 + F_2 \\ \boldsymbol{M}_0 &= \boldsymbol{p} \times \boldsymbol{F}_0 + \boldsymbol{M}_p \\ &= \boldsymbol{M}_{01} + \boldsymbol{M}_{02} \\ &= \boldsymbol{p}_1 \times \boldsymbol{F}_1 + \boldsymbol{M}_{p1} + \boldsymbol{p}_2 \times \boldsymbol{F}_2 + \boldsymbol{M}_{p2} \end{aligned} \tag{5}$$

where $\boldsymbol{M}_{01}^\top = (M_{1x}, M_{1y}, M_{1z})^\top$ and $\boldsymbol{M}_{02}^\top = (M_{2x}, M_{2y}, M_{3z})^\top$, are the moment exerted by the contact on leg 1 and 2 expressed in the global frame Σ_0 (see figure 3) while $\boldsymbol{M}_{p1}$, $\boldsymbol{M}_{p2}$ are the moment expressed in frame centered in p_1 and p_2. By considering that $(\boldsymbol{F}_0, \boldsymbol{M}_p)^\top = (F_x, F_y, F_z, 0, 0, M_z^*)^\top$, $(\boldsymbol{F}_1, \boldsymbol{M}_{p1})^\top = (F_{x1}, F_{y1}, F_{z1}, 0, 0, M_{z1}^*)^\top$, and $(\boldsymbol{F}_2, \boldsymbol{M}_{p2})^\top = (F_{x2}, F_{y2}, F_{z2}, 0, 0, M_{z2}^*)^\top$, the position of the global ZMP can be deduced as follows:

$$\begin{aligned} p_x &= \frac{p_{1x} F_{1z} + p_{2x} F_{2z}}{F_{1z} + F_{2z}} \\ p_y &= \frac{p_{1y} F_{1z} + p_{2y} F_{2z}}{F_{1z} + F_{2z}} \end{aligned} \tag{6}$$

Let us remark that, a desired global ZMP trajectory is imposed by using the essential model, then, by defining a local ZMP for each foot, forces F_{1z} and F_{2z} can be deduced from (6)

4.2 Dynamic model of *Romeo* with explicit unilateral constraint with the ground

Let Σ_0 be the world frame, whose origin is located in the center of a foot with a foot-flat contact on the ground. The dynamic model of the humanoid robot (see [2]) can be written with both following matrix equations:

$$\begin{pmatrix} F_0 \\ M_0 \end{pmatrix} = \begin{pmatrix} A_F \\ A_M \end{pmatrix} \ddot{q} + \begin{pmatrix} d_F(q, \dot{q}) \\ d_M(q, \dot{q}) \end{pmatrix}, \tag{7}$$

$$\tau = A\ddot{q} + d(q, \dot{q}). \tag{8}$$

where, for the case of *Romeo*, $q \in \mathbb{R}^{31\times 1}$ is the introduced joint vector in subsection 3.1, $\tau \in \mathbb{R}^{31\times 1}$ is the joint torque vector, $A_F \in \mathbb{R}^{3\times 31}$, $A_M \in \mathbb{R}^{3\times 31}$, $A \in \mathbb{R}^{31\times 31}$ is the inertia matrix of the humanoid robot, $d_F \in \mathbb{R}^{3\times 1}$, $d_M \in \mathbb{R}^{3\times 1}$ and $d \in \mathbb{R}^{31\times 1}$ are vectors that represent Coriolis, centrifugal, gravity effects and the wrench ground reaction acting on the other foot in double support phase. The matrix equation (7) defines the global equilibrium of the robot, which can be written in the frame Σ_0.

4.3 Presentation of the Essential model

Instead of imposing as many trajectories as the number of DoF, the principle of *Essential model* is to let free two DoF to allow for a chosen placement of the ZMP. The relation between ZMP and CoM is considered to be a determining feature of human gait [4], [6], and they are strongly linked. The horizontal coordinates of the CoM, defined as $r_f = (x, y) \in \mathbb{R}^{1\times 2}$, are chosen to be "free" in order to adapt them to the imposed trajectory of the ZMP.

The complete motion of the humanoid robot is defined by

$$\begin{aligned} r &= (r_f, r_c)^\top \\ &= (x, y, z(t), x_f(t), y_f(t), z_f(t), \psi_f(t), \theta_f(t), \\ &\quad \phi_f(t), \psi_t(t), \theta_t(t), \phi_t(t), q_{13}(t), \cdots, q_{31}(t))^\top. \end{aligned} \tag{9}$$

where $r \in \mathbb{R}^{31\times 1}$. Vector $r_c \in \mathbb{R}^{1\times 29}$ is defined as the vector of the 29 following variables of r for which the trajectories are imposed. The desired altitude of the CoM is described by $z(t)$. $x_f(t), y_f(t), z_f(t)$ and $\psi_f(t), \theta_f(t), \phi_f(t)$ describe the desired position and orientation of the swing foot, meanwhile, ψ_t, θ_t, ϕ_t the desired orientation of the torso link. The upper-body joint motions are described by q_{13} to q_{31}. The desired trajectory for $r_c(t)$ is therefore defined based on gross averaged characteristics of human motion.

The robot configuration can be defined by the joint vector $q \in \mathbb{R}^{31\times 1}$ or by the vector $r \in \mathbb{R}^{31\times 1}$, and a geometric model $q = g(r_f, r_c)$ can be built. The vectors $\dot{q} \in \mathbb{R}^{31\times 1}$ and $\ddot{q} \in \mathbb{R}^{31\times 1}$ are deduced thanks to the kinematic models as follows:

$$\dot{q} = J_f \dot{r}_f + J_c \dot{r}_c, \quad \ddot{q} = J_f \ddot{r}_f + \dot{J}_f \dot{r}_f + J_c \ddot{r}_c + \dot{J}_c \dot{r}_c. \tag{10}$$

Here $J_f = \dfrac{\partial g}{\partial r_f} \in \mathbb{R}^{31\times 2}$ and $J_c = \dfrac{\partial g}{\partial r_c} \in \mathbb{R}^{31\times 29}$. In this study the evolution of $r_c \in \mathbb{R}^{29\times 1}$ is chosen as a function of time, thus the joint evolution can be expressed as function of $r_f, \dot{r}_f, \ddot{r}_f$, and t only :

$$\begin{aligned} q = g(r_f, r_c(t)), \quad \dot{q} = J_f \dot{r}_f + v(t, r_f), \\ \ddot{q} = J_f \ddot{r}_f + \dot{J}_f \dot{r}_f + a(t, r_f, \dot{r}_f), \end{aligned} \tag{11}$$

where $v(t, r_f) = \frac{\mathrm{d}g(r_f, r_c(t))}{\mathrm{d}t} \in \mathbb{R}^{31\times 1}$ and $a(t, r_f, \dot{r}_f) = \frac{\mathrm{d}^2 g(r_f, r_c(t))}{\mathrm{d}t^2} \in \mathbb{R}^{31\times 1}$.

By using (11), the global equilibrium (7) can be rewritten as

$$\begin{pmatrix} \boldsymbol{F}_0 \\ \boldsymbol{M}_0 \end{pmatrix} = \begin{pmatrix} A_{Fr}(t, r_f) \\ A_{Mr}(t, r_f) \end{pmatrix} \ddot{r}_f + \begin{pmatrix} d_{Fr}(t, r_f, \dot{r}_f) \\ d_{Mr}(t, r_f, \dot{r}_f). \end{pmatrix} \tag{12}$$

On the other hand, system (4) with the wrench $W_0 = (\boldsymbol{F}_0, \boldsymbol{M}_0)^\top$ can be rewritten as:

$$\begin{pmatrix} 0 & 0 & p_x(t) & 0 & 1 & 0 \\ 0 & 0 & p_y(t) & -1 & 0 & 0 \end{pmatrix} W_0 = \begin{pmatrix} 0 \\ 0 \end{pmatrix}. \tag{13}$$

During the SS phase the desired motion of the ZMP defined by $p_x(t)$ and $p_y(t)$ is chosen as a migration from the heel to the toe of the stance foot. In DS phase the desired motion of the ZMP is defined by a linear evolution from the final position of the ZMP at the end of the SS phase on the stance foot, to the initial position of the ZMP at the beginning of the SS on the next stance foot. Considering the 3^{rd}, 4^{th},

and 5^{th} lines of (12), which are respectively relative to F_z, M_x, and M_y, and taking into account the relations (4), the two following differential equations can be deduced:

$$\begin{aligned}\left(A_{Frz}(t,r_f)p_x(t) + A_{Mry}(t,r_f)\right)\ddot{r}_f + d_{Frz}(t,r_f,\dot{r}_f)p_x(t) + d_{Mry}(t,r_f,\dot{r}_f) = 0,\\ \left(A_{Frz}(t,r_f)p_y(t) - A_{Mrx}(t,r_f)\right)\ddot{r}_f + d_{Frz}(t,r_f,\dot{r}_f)p_y(t) - d_{Mrx}(t,r_f,\dot{r}_f) = 0.\end{aligned} \tag{14}$$

The two scalar equations (14) isolate the essential characteristic of the walking that is the relationship between the ZMP and the CoM. Solving (14) gives the *Essential model* that describes the acceleration of the horizontal positions $r_f = (x, y)$ of the CoM as function of the desired evolution of the ZMP:

$$\ddot{r}_f = f(r_f, \dot{r}_f, t, p_x(t), p_y(t)). \tag{15}$$

Then, the velocities $\dot{r}_f = (\dot{x},\ \dot{y})$, and positions $r_f = (x, y)$ of the CoM can be calculated by integrating (15) from some known initial conditions. To sum up, the evolution of $r_f = (x, y)$ is not imposed, but computed to adapt it to the desired evolution $p_x(t)$, $p_y(t)$ of the ZMP. Let us remark that, with this strategy, no approximations are made to the dynamic model of the robot, when designing the humanoid walking. Therefore, this method ensures the feasibility of a walking trajectory such as it was designed, since it comes from the equilibrium condition on the ZMP (4).

4.4 Validation of the Constraints of contact with the ground

By definition the essential model allows to satisfy *a priori* the following constraints:

- The ZMP within the sustentation polygon for all time.
- The positivity of the vertical component of the resultant ground reaction force during the walking (no lift-off condition) by choosing a convenient trajectory of the CoM height $z(t)$. It is sufficient that $z(t)$ satisfies:

$$\ddot{z}(t) > -g. \tag{16}$$

When the walking motion is defined it is necessary to check *a posteriori* that:

- The no-slip constraint and the technological constraint of actuator limitation are satisfied. The condition of no slipping can be checked based on the knowledge of $\ddot{r}_f$ and $\ddot{z}$. It is sufficient to satisfy:

$$\|\ddot{r}_f\| < \mu\|\ddot{z}(t) + g\|. \tag{17}$$

- The joint velocity $\dot{q}(i)$ within the maximum velocity allowed by each motor $\dot{q}_{\max}(i)$, for $i = 1, \cdots, 31$:

$$|\dot{q}(i)| < \dot{q}_{\max}(i) \tag{18}$$

- The joint torque $\tau(i)$ within the maximum torque allowed by each motor $\Gamma_{\max}(i)$, for $i = 1, \cdots, 31$:

$$|\tau(i)| < \Gamma_{\max}(i) \tag{19}$$

In reality, especially with electric motors, constraints (18) and (19) are not independent. During the experimental tests, care must be taken to ensure that at all times for each motor i the motor limit, which depends on both speed and torque, is never exceeded. For *Romeo*, the maximal torque for the knee Γ_{max} depends on the knee position.

4.5 Diagram of the walking design, which is based on the human-inspired trajectories and the *Essential Model*

To introduce the scheme of Fig. 4, several relations are recalled. First, the global equilibrium (7) can be rewritten as

$$W_0 = P^{\omega}\ddot{q} + \lambda^{\omega}. \tag{20}$$

with $W_0 = \begin{pmatrix} \boldsymbol{F}_0 \\ \boldsymbol{M}_0 \end{pmatrix} \in \mathbb{R}^{6\times 1}$, $P^{\omega} = \begin{pmatrix} A_F \\ A_M \end{pmatrix}^{\top} \in \mathbb{R}^{6\times 31}$, and $\lambda^{\omega} = \begin{pmatrix} d_F(q,\dot{q}) \\ d_M(q,\dot{q}) \end{pmatrix} \in \mathbb{R}^{6\times 1}$.

By using the direct geometric model, the first and second kinematic models can be obtained as

$$\begin{cases} r = g(q) \\ \dot{r} = J_g(q)\ \dot{q} \\ \ddot{r} = J_g(q)\ \ddot{q} + \dot{J}_g(q,\dot{q})\ \dot{q}. \end{cases} \tag{21}$$

Then, by solving the second kinematic model for $\ddot{q}$, the second inverse kinematic model is deduced, *i.e.*:

$$\ddot{q} = P^{IKM}\ddot{r} + \lambda^{IKM}, \tag{22}$$

where $P^{IKM} = J_g^{-1}(q) = \left(\dfrac{\partial J_g}{\partial q}\right)^{-1} \in \mathbb{R}^{31\times 31}$ and $\lambda^{IKM} = -J_g^{-1}(q)\dot{J}_g(q,\dot{q})\ \dot{q} \in \mathbb{R}^{31\times 31}$.

To summarize the *essential model* can be illustrated by the input/output scheme 4. The inputs are the trajectory of the ZMP and the reference trajectory of each component of the vector r_c. By considering the equilibrium of the moments of the ground reaction, the dynamic equilibrium, the unilateral constraints, the geometrical and kinematic relations between r, $\dot{r}$ and q, $\dot{q}$, the horizontal evolution r_f of the CoM is computed. *In fine* the knowledge of q, $\dot{q}$, and $\ddot{q}$ allows to evaluate the joint torques and thus *a postiori* to check if the motor constraints are satisfied. The outputs of this model are used to define the control, which can be based for example on a nominal vector torque with correction in joint position and velocity or a computed torque control with an auxiliary input to ensure a trajectory tracking.

4.6 Torques and ground forces in SS and DS

The torques required to produce the motion have to be calculated. By considering the matrix equation (8) and relations (11), the dynamic behavior of the robot in the SS phase can be written as

$$\tau = A_r(t, r_f)\ddot{r}_f + d_r(t, r_f, \dot{r}_f) \tag{23}$$

where $A_r(t, r_f) \in \mathbb{R}^{31\times 2}$ and $d_r(t, r_f) \in \mathbb{R}^{31\times 1}$.
In DS phase, the equation of equilibrium (8) can be used to obtain the global reaction wrench $\boldsymbol{F}_0$, $\boldsymbol{M}_0$, but the distribution on both legs is free to choose. However, this choice will modify the actuation torque. If the effort wrench applied on the second leg is non-zero and is denoted $(F_{ext}, M_{ext})^{\top}$, the joint torque are modified and becomes:

$$\tau = A_r(t, r_f)\ddot{r}_f + d_r(t, r_f, \dot{r}_f) + J_{ext}^{\top}\begin{pmatrix} F_{ext} \\ M_{ext} \end{pmatrix}, \tag{24}$$

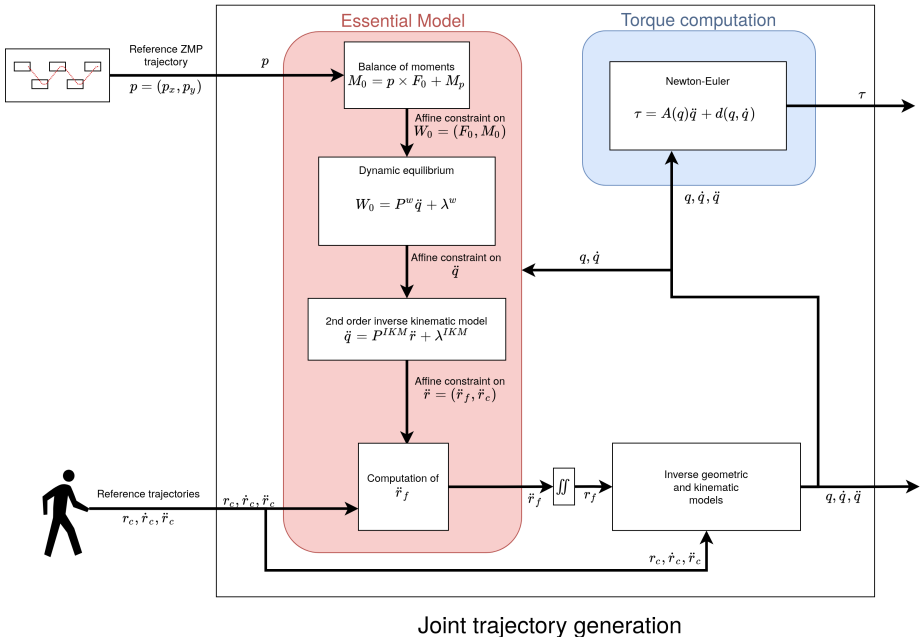

Joint trajectory generation

Fig. 4: How the generation of human-inspired trajectories using the *Essential Model* works

with $J_{ext} \in \mathbb{R}^{6\times 31}$ as the Jacobian matrix that relates the frame on the sole swing foot with the origin Σ_0. In order to determine the distribution of the global reaction wrench $\boldsymbol{F}_0$, $\boldsymbol{M}_0$ on the two feet, we will impose the positions of local ZMP in both feet, defined as p_1 and p_2. During a DS, the global ZMP is the barycenter of the two local ZMP on each foot, this implies that the global ZMP and the local ZMP are aligned. In DS, the choice of local ZMP p_1 and p_2 is used to calculate the distribution of efforts. This choice must limit the internal forces useless to the motion in order to avoid increasing the joint torques. Then the vertical reaction force F_{1z} and F_{2z} on legs 1 and 2 can be calculated by solving (6).

$$\begin{aligned} \frac{p_{1x}F_{1z} + p_{2x}F_{2z}}{F_{1z} + F_{2z}} &= p_x \\ \frac{p_{1y}F_{1z} + p_{2y}F_{2z}}{F_{1z} + F_{2z}} &= p_y \end{aligned} \tag{25}$$

To limit the risk of slipping, the ratio between tangential and normal forces for the global equilibrium is chosen equal for each leg. The components F_{1x}, F_{1y}, F_{2x}, and F_{2y} are calculated to satisfy:

$$\begin{aligned} \frac{F_{1x}}{F_{1z}} = \frac{F_{2x}}{F_{2z}} = \frac{F_{1x} + F_{2x}}{F_{1z} + F_{2z}} = \frac{F_x}{F_z} \\ \frac{F_{1y}}{F_{1z}} = \frac{F_{2y}}{F_{2z}} = \frac{F_{1y} + F_{2y}}{F_{1z} + F_{2z}} = \frac{F_y}{F_z} \end{aligned} \tag{26}$$

By using (5) it is possible to find the moment M_z around the z axis

$$M_z = M_{1z} + M_{2z}$$

This moment M_z is also shared between the two legs by using a similar distribution to the force components (26) as follows:

$$\frac{M_{1z}}{F_{1z}} = \frac{M_{2z}}{F_{2z}} = \frac{M_{1z} + M_{2z}}{F_{1z} + F_{2z}} = \frac{M_z}{F_z}. \tag{27}$$

In this study, two types of DS phases are considered.

- DS during the walking motion which allow to join two phases of SS with foot position offsets along both x and y axes. We want to have a continuous evolution of the ZMP, which results in continuous joint torques and avoids high jerk. We choose an evolution of the global ZMP such that, during the DS phases, the two local ZMP keep a constant pose. According to experimental data [20], the centre of pressure under the foot during human walking moves continuously from the heel to the forefoot. The centre of pressure moves slowly forward in the region immediately in front of the heel while it accelerates as it approaches the forefoot before the foot lifts. However, since the robot's foot is flat on the ground, it will be assumed that the local ZMP remains constant during the double support. In addition, it allows a simple and rigorous calculation of the evolution of the global ZMP in DS. p_1 will keep the pose corresponding to the final pose of the global ZMP in SS, meanwhile p_2 will keep the initial pose of the ZMP for the next SS phase. The global ZMP evolves in a straight line between the final pose of the ZMP during the previous SS and the initial pose of the ZMP during the next SS.
- For the initial DS in the starting phase, or the final DS in the stopping phase, on the contrary, the humanoid robot has the two feet aligned along the x-axis. Therefore, a non-straight line evolution of the global ZMP is needed [31], which means that the two local ZMP cannot be static. The local ZMP will then be chosen to yield the current value of the global ZMP along the x-axis while remaining within the surface of the corresponding foot. A linear ZMP evolution along the y-axis is chosen. The aim is to ensure continuity and to minimize the lateral torque on the ankle. An illustration is shown in Fig. 11 for the case studied. In addition, when stationary, we want an identical distribution of forces over the two feet. Thus, at the beginning of DS_1 and the end of DS_n, we choose a median ZMP position between the two feet along the y-direction. The two local ZMP are respectively on the y-median-position of each foot, Fig. 12.

5 Periodic walking motion

The periodic motion is composed of SS phases and DS phases with flat foot contacts on the ground. The orientation of the swing foot varies during the SS phase. During DS phases the contacts are made with the feet flat on the ground. Sinusoidal functions are used to define the motions of the arms and the trunk. The parameters of these functions are tuned based on observations of human motions [32] and in section 3.2.

To find the periodic motion, a boundary value problem is stated and solved as follows. Let $(r_f(t_0), \dot{r}_f(t_0))^\top$ be the horizontal plane of the position and velocity of the

CoM at the beginning of a current step of the walking motion. The periodic condition is

$$(r_f(t_0), \dot{r}_f(t_0))^\top = (r_f(t_0+T), \dot{r}_f^+(t_0+T)^\top \tag{28}$$

by taking into account the change of the reference frame when the two legs switch their roles just at the beginning of the current step. So $\dot{r}_f^+(t_0+T)$ is the initial horizontal velocity of CoM in SS of the next step. Let the following state model of equation (15) be used

$$\begin{aligned} \dot{\mathbf{x}}_1 &= \mathbf{x}_2 \in \mathbb{R}^2 \\ \dot{\mathbf{x}}_2 &= f(\mathbf{x}_1, \mathbf{x}_2, t, p_x(t), p_y(t)), \end{aligned} \tag{29}$$

with $\mathbf{x}_1 = r_f$ and $\mathbf{x}_2 = \dot{r}_f$. The boundary value problem is stated as: what are the **four** unknown variables $x(t_0)$, $y(t_0)$, $\dot{x}(t_0)$ and $\dot{y}(t_0)$ such that after integration of the **four** scalar equations (29) over the time interval $[t_0, t_0+T]$ the periodic condition (28) is satisfied. The *fsolve* function of Matlab ® is used to solve numerically the boundary value problem described above.

6 Starting and stopping of walking motion

In order to perform the target periodic walking motion experimentally, it is necessary to add starting and stopping motions, which are composed of DS and SS phases. This allows the robot to start from (resp. to stop in) a resting position. Each resting position is defined to be a static equilibrium where the vertical projection of the CoM on the ground is merged with the ZMP close to the center of the support area. The chosen ZMP trajectory takes inspiration from what is observed in human walking [20] and is defined using piecewise polynomial functions to be adapted to a humanoid robot. A sequence of a starting motion (DS_1, SS_1, and DS_2), a periodic walking motion (SS and DS) and a stopping motion (SS_{n-1}, DS_{n-1}, SS_n, and DS_n) is shown in Fig. 5.

The starting motion begins with a DS_1 phase, with both feet aligned in the frontal plane. During this DS, *Romeo* swings to the right in order to lift the left foot and begin a SS_1 phase on its right foot. At the end of this SS_1 phase *Romeo* performs another DS_2 phase in order to reach the periodic walking motion at the end of this motion. For the starting of the walking motion, the following "control points" are introduced:

- $\mathbf{P_0}$ ZMP at the start of DS_1,
- $\mathbf{P_1}$ ZMP in the middle of DS_1,
- $\mathbf{P_2}$ ZMP at the transition between DS_1 and SS_1,
- $\mathbf{P_3}$ ZMP at the transition between SS_1 and DS_2,
- $\mathbf{P_4}$ ZMP at the end of the DS_2 phase.

These control points are used to define the evolution of ZMP during starting phase. They are illustrated on Fig. 5.

Let p_x and p_y be the evolution of the ZMP position along the x-axis and y-axis respectively. In DS_1 phase, p_x and p_y are both defined as quadratic functions of time going from $\mathbf{P_0}$ to $\mathbf{P_2}$ with the intermediate point $\mathbf{P_1}$. In SS_1 and DS_2 phases p_x and p_y are defined as linear functions of time connecting, respectively, $\mathbf{P_2}$ to $\mathbf{P_3}$ and $\mathbf{P_3}$ to $\mathbf{P_4}$. $\mathbf{P_4}$ is imposed by the chosen periodic trajectory.

The stopping motion begins with a phase of simple support SS_{n-1}, to put the left foot in its final position. At the end of this SS_{n-1} a double support phase DS_{n-1}

begins. At the end of this DS_{n-1} phase, the right foot is swing. The last single support is SS_n. At the end of this SS_n phase, the right foot is aligned with the left foot in the frontal plane. Finally, the stopping movement ends with the DS_n phase in order to superimpose the ZMP with the projection of the CoM on the ground and thus immobilize the bipedal robot. For the stopping of the walking motion, the strategy to define the ZMP trajectory is similar to the previous one. We define:

- $\mathbf{P_5}$ ZMP at the transition between SS_{n-1} and DS_{n-1},
- $\mathbf{P_6}$ ZMP at the transition between DS_{n-1} and SS_n,
- $\mathbf{P_7}$ ZMP at the transition between SS_n and DS_n,
- $\mathbf{P_8}$ ZMP in the middle of DS_n,
- $\mathbf{P_9}$ ZMP at the end of the DS_n phase.

At the start of SS_{n-1} phase, the ZMP position is (taking into account the change of reference frame) the same as in $\mathbf{P_4}$ because of the periodic nature of the trajectory before SS_{n-1}. We can therefore denote this point as $\mathbf{P_4}$ as well. In SS_{n-1} phase, p_x and p_y are therefore defined as linear functions to connect $\mathbf{P_4}$ to $\mathbf{P_5}$. In DS_{n-1} and SS_n phases, p_x and p_y are defined as linear functions of time to connect $\mathbf{P_5}$ to $\mathbf{P_6}$, $\mathbf{P_6}$ to $\mathbf{P_7}$, respectively. In DS_n phase p_x and p_y are defined as quadratic functions of time connecting $\mathbf{P_7}$ to $\mathbf{P_9}$ with an intermediate point $\mathbf{P_8}$ which is chosen in the middle between the two feet along y-axis.

The stopping phase with two DS phases and two SS phases is not symmetric with respect to the starting phase with two DS phases and only one SS phase. This asymmetry is due to the fact that the steady-sate gait is not one-step capturable. The step width D and the step length S are given but not necessarily equal between the starting, stopping and periodic motions. Boundary value problems are solved to define the starting and stopping motions which are stated as follows:

Starting motion Let us consider the known two coordinates of the horizontal position of the CoM, which is also the ZMP position $\mathbf{P_0}$. The two horizontal velocities of the CoM are equal to zero. Let us consider the known **two** coordinates of the horizontal position of the CoM at the end of DS_2 phase and their two velocities. These two coordinates and **two** velocities are also the state of the periodic horizontal motion of the CoM at the beginning of the SS phase.
Let us take into account the essential model (29) and the duration of the starting motion T_{start}. What are the **four** possible variables to carry out the starting motion by integration of (29) from the starting state

$$(r_f(0), \dot{r}_f(0))^\top \tag{30}$$

of the CoM, to the final state

$$(r_f(T_{start}), \dot{r}_f(T_{start}))^\top. \tag{31}$$

of the starting motion. We choose x-axis and y-axis components of the two *control points* $\mathbf{P_2}$, and $\mathbf{P_3}$ of the ZMP trajectory, to solve the boundary value problem. A SQP method (Sequential Quadratic Programming) with *fmincon* of Matlab ® is used to find the **four** unknown variables, which correspond to the two coordinates of $\mathbf{P_2}$, and $\mathbf{P_3}$ respectively, with constraints for the support area limits in order to ensure that the ZMP is always inside of the support area. The final state (31) is compared to the target state

$$(r_f^{des}(T_{start}), \dot{r}_f^{des}(T_{start}))^\top \tag{32}$$

by using a Mean Square criterion (optionally weighed to emphasize the importance of one of the dimensions):

$$J = \|(r_f(T_{start}) - r_f^{des}(T_{start}))^\top\|^2 + \|(\dot{r}_f(T_{start}) - \dot{r}_f^{des}(T_{start}))^\top\|^2. \quad (33)$$

The boundary value problem used to find the starting walking motion is solved when the criterion J (33) is equal to zero and the trajectory of the ZMP is inside of the convex hull of the support area.
Remark : In practice, starting from the need to have coincident between CoM and ZMP in statics and identical but opposite directions of speed, using the knowledge of the movement of the CoM for the starting phase of human walking and the knowledge of the relationship between the evolution of the CoM and the ZMP on a LIP model, an *a priori* choice of the positions of the points P_1, P_2, P_3, is made. Then the positions of the points P_1, P_2, P_3 are refined by optimization with the criterion (33). This criterion admits an infinite number of minima and does not converge very well. Also this first optimization is used to bring us the criterion towards a weak value then the positions of the points P_1 is frozen to switch on a problem of boundary conditions with four variables to be optimized to cancel four error of state that converges better.

Stopping motion The strategy is similar to that of the starting motion. Then to carry out the stopping of the walking motion we choose the x-axis and y-axis components of the two control points $\mathbf{P_6}$ to $\mathbf{P_7}$ of the ZMP trajectory as the **four** unknown variables to solve this boundary problem. The **four** scalar equations represented by (29) are then integrated from the final state of the periodic motion $(r_f(T_{end}), \dot{r}_f(T_{end}))^\top$ for the CoM, to the stop state $(r_f(T_{stop}), \dot{r}_f(T_{stop}))^\top$. The desired stop state is $(r_f^{stop}, \mathbf{0})^\top$. An equivalent criterion to (33) is calculated with respect to the **two** coordinates of the horizontal resting position of the CoM and their

$$J = \|(r_f(T_{stop}) - r_f^{stop})^\top\|^2 + \|\dot{r}_f(T_{stop})^\top\|^2. \quad (34)$$

This boundary value problem defining the stop the walking motion is solved when the criterion J (34) is equal to zero and the trajectory of the ZMP is inside of the convex hull of the support area. The same SQP method (Sequential Quadratic Programming) with *fmincon* of Matlab ® is also used to find the solution of (34).

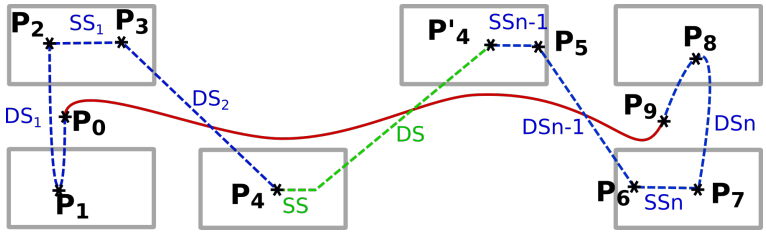

Fig. 5: Sequence of starting motion (blue), periodic walking gait (green) and stopping motion (blue).

All joint trajectories also need to be continuous during this transition. And since there is no impact in our gait, this is equivalent to impose that the evolution of r_c be continuous. The sinusoidal functions, which define the actuated joints of the arms and trunk, are multiplied by a piecewise polynomial cut-off function which is equal to 1 during the periodic motion and first and second derivatives smooth goes to 0 during the starting and stopping phases in order to start and to stop with a null velocity and null acceleration.

7 Numerical results

7.1 Periodic motion, without the use of the *Essential model*

We use all adapted parameters (see section 3.2) and a sinusoidal evolution of the COM that is equivalent to the human COM trajectory. The trajectory is therefore completely defined without the use of the Essential Model. As expected, the ZMP trajectory is outside the support polygon, see Fig. 6.

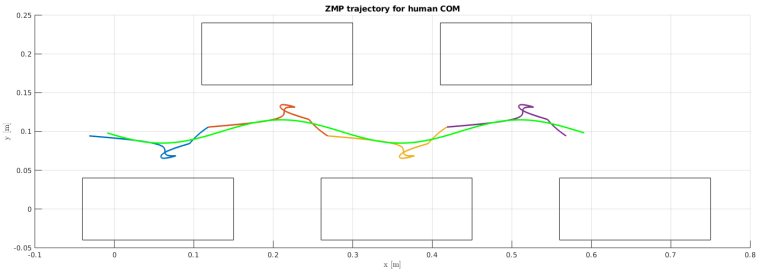

Fig. 6: In the horizontal plane (defined with the X-abscissa and Y-ordinate axes): ZMP (multicolored) obtained if the human CoM (x, y, z) motion (in green) and adapted trajectories are applied to the robot *Romeo*.

7.2 Periodic motion by using *Essential model*

We choose a ZMP trajectory close to the one that is observed in humans. Since we do not have foot roll-off motion, we avoid the ZMP reaching the edges of the foot. That way, the non-tilting condition is safely satisfied.

The evolution of ZMP in DS phase is chosen as follows:

- In x-direction, from $p_x = 0$ (under the ankle) to $p_x = 0.10$m (near the foot toes).
- In y-direction, $p_y = 0$ (center of the foot).

The corresponding CoM trajectory is represented on Fig. 7. We observe that the CoM trajectory in the horizontal plane is not far from a sinusoidal function, which is what is observed for humans [17].

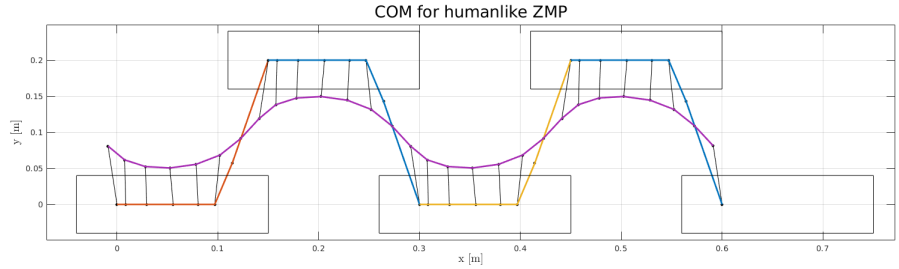

Fig. 7: CoM trajectory (purple) corresponding to a human-like evolution of the ZMP (multicolor).

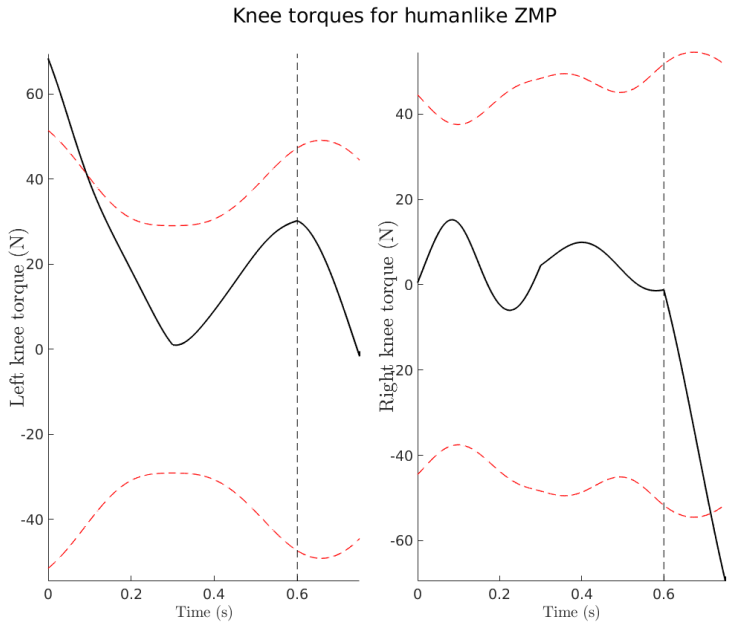

Fig. 8: Torques (solid line) at both knees for a human-like ZMP trajectory. The dashed line marks the end of the SS phase (swing foot contact), and the red dashed lines show the maximal acceptable torque for *Romeo*. It is interesting to remark that these limits are not constant - this is because of a specificity of the knee joint in *Romeo*: the maximum torque depends on the joint position. The required torque at the beginning of SS is higher than the torque limit.

However, when calculating the torque values for this trajectory, we observe that for one step, which consists of a SS phase with the left leg as the stance leg and a DS phase the torques at the knees are not compatible with the hardware of *Romeo*, as shown in Fig. 8. In SS phase the left leg is the stance leg. In order to reduce these torques,

we need to modify some of the original parameters. We analyzed the effect of various parameters on the torques, and observed that the most efficient way to influence the knee torques is to modify the ZMP trajectory. The result is presented in the following section, and the trajectory used in the rest of the paper is the modified one.

7.3 Effect of ZMP evolution on torques

The results presented above correspond to an evolution of the ZMP going from the heel to the tip of each foot (see Fig. 7). The torque at the ankle is directly affected by the pose of the ZMP. It can be seen in Fig. 9 (2^{nd} picture), that the propulsive torque at the ankle is low at the beginning of the step. As a consequence, a high propulsive torque is required at the knee joint (Fig. 9 (3^{rd} picture)). In fact this high torque exceeds the limits of the actuator (shown in dotted line) of the robot *Romeo*. We explored the effect of the influence of ZMP evolution. The results consistently confirm that a modification of the ZMP trajectory influences the torques in the support knee and in the support ankle. A ZMP whose position evolves on the front of the foot allows a higher propulsive force in the ankle at the beginning of the SS, and thus allows to decrease the propulsive force at knee, and then a suitable torque for the knee actuator of *Romeo* is obtained.

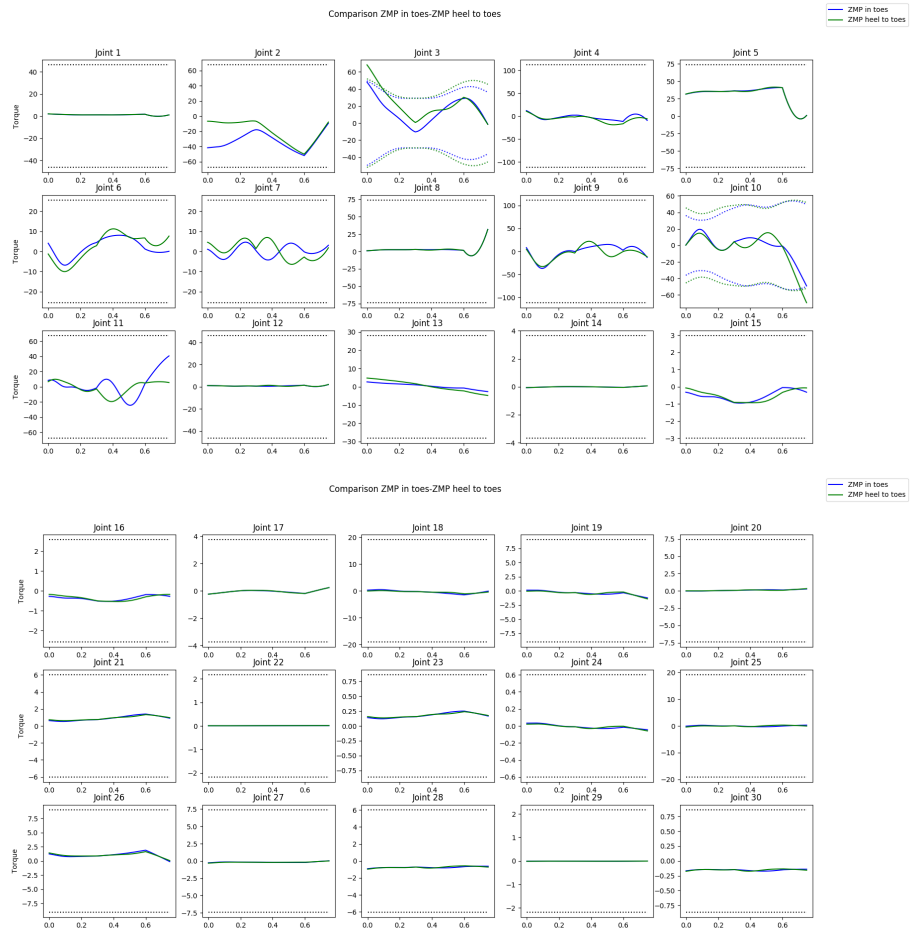

Fig. 9: Joint torques (N.m) versus time (s): comparison of the torque in the lower part of the robot for two periodic trajectories with a step size of 0.20 m and a period of 0.75 s. The trajectory in green is with a human like ZMP evolution in DS, and the trajectory in blue has a ZMP constrained to the front of the foot. The dashed lines represent the maximal acceptable torque for Romeo.

7.4 Complete motion

A video simulation of the complete walking trajectory is available here. The synthesized walking trajectory is such that the step width parameter D is the same for the starting, periodic and stopping motions. The step length parameter S is chosen to be 0.16 m, 0.15 m and 0.20 m for the starting, periodic and stopping motions respectively. For this synthesized trajectory, the trajectories of the horizontal position of the CoM and the determined trajectory of the ZMP are shown Fig. 10. The starting motion and the stopping phases are respectively composed of three and four phases, see Fig. 5.

Four steps make up the periodic motion. We can observe that the CoM and ZMP evolutions are continuous from the starting to the stopping configuration.

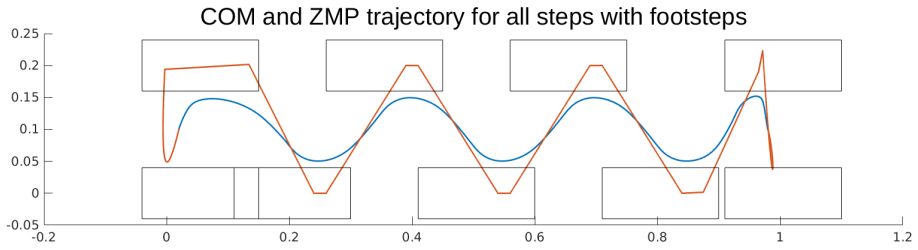

Fig. 10: Imposed ZMP trajectory (orange) and corresponding CoM (blue). The dashed rectangles represent the foot placements.

A focus of the starting and stopping motions is shown in Fig. 11. The horizontal position of the CoM and the ZMP position match at the starting and stopping configurations. The control points to solve the two boundary value problems are depicted with green stars.

In the first phase DS_1 and last DS_n phase, the ZMP follows a more complex trajectory. It is therefore necessary to define a non-constant local ZMP for each foot. We choose at each moment to have the same x coordinate for both the local ZMP and the global ZMP. Each local ZMP must remain as close as possible to the center of each foot in the y direction to improve the stability of the walk. Continuity between the position of the ZMP at the end of DS_1 and the position of the ZMP at the beginning of the single-support phase SS_1 must be ensured in $\mathbf{P}_2$, and continuity between the position of the ZMP at the beginning of DS_n and the position at the end of the single-support phase SS_n must be ensured in $\mathbf{P}_7$, respectively. The resulting local ZMP trajectories are presented in Fig. 12.

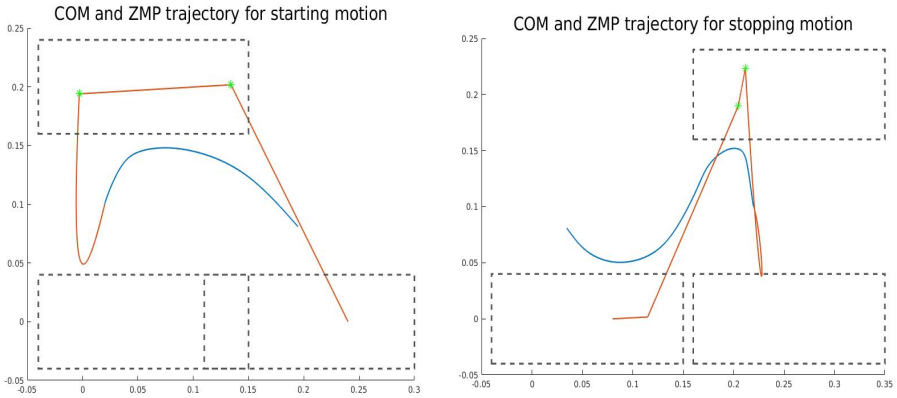

a b

Fig. 11: Imposed ZMP trajectory (orange) and horizontal position of the corresponding CoM (blue) during the starting (a) and the stopping motions (b). The dashed rectangles represent the outlines of the feet on the ground.

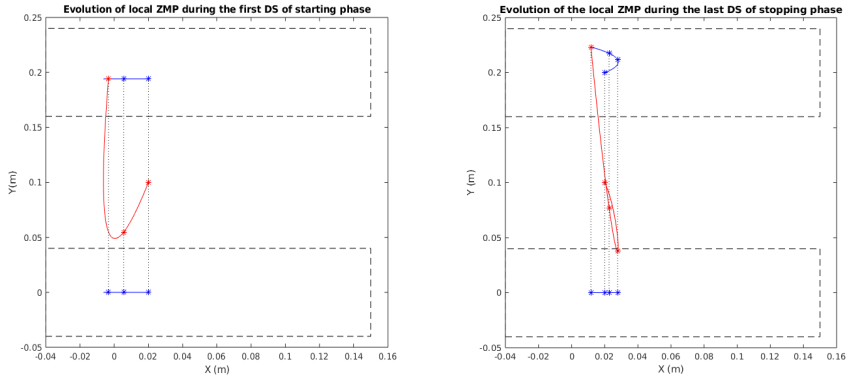

a b

Fig. 12: Evolution of the local ZMP (blue) for each foot respectively during the first and last DS phases of the starting (a) and stopping (b) motions. The dashed lines show the distribution of the global ZMP and the alignment at all times between the two local ZMPs and the global ZMP (red).

We can also verify that the non slipping condition is fulfilled. This condition is that the ratio between the tangential and normal forces does not exceed the friction coefficient (see Fig. 13). This friction coefficient is chosen equal to 0.7 here. Both of these forces are calculated with (20). The sinusoidal-like shape of the normal reaction force observed in Fig. 13 is linked to the oscillations of the height z the CoM, *i.e.* $F = m\ddot{z} + mg$.

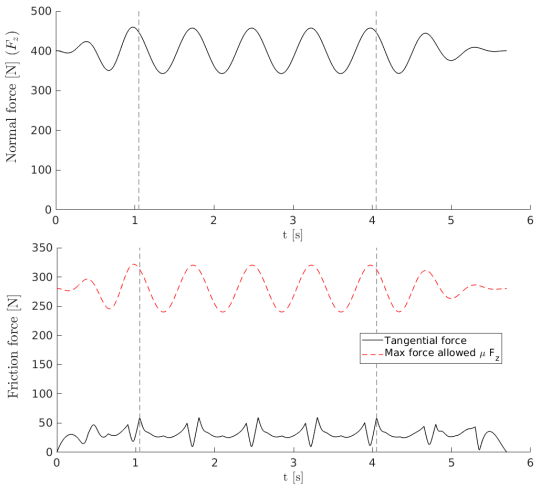

Fig. 13: F_z Normal (top plot) and $\|F_x + F_y\|$ tangential (bottom) components of the reaction force F_0. The red dashed line represents the maximum acceptable tangential force without risk of slipping.

We compute the torque value for all of the joints. However, we choose to only present in Fig. 14 the joint torques in the sagittal plane of both legs. Indeed, these are the torques that require the highest magnitude. It can be observed (blue curves in figure 9) that the torques are within the motor limits for *Romeo*. The torques required for starting, periodic, and stopping motions are of similar magnitude as what is required for periodic motion.

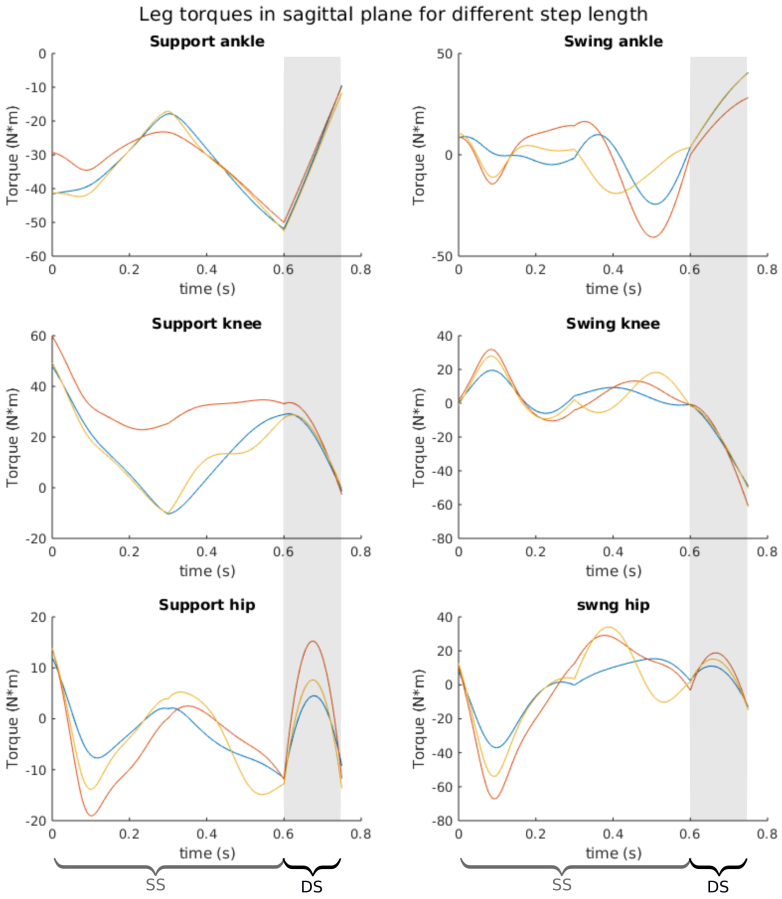

Fig. 14: The torque at the ankle, knee, and hip joints, in the sagittal plane for different periodic motions with a step width of 0.20: step length 0.15m (blue), 0.20m (yellow) and 0.30m (red). A single step is represented. From time t = 0s to t=0.6s is the SS phase, from t=0.6s to 0.75s is the DS phase.

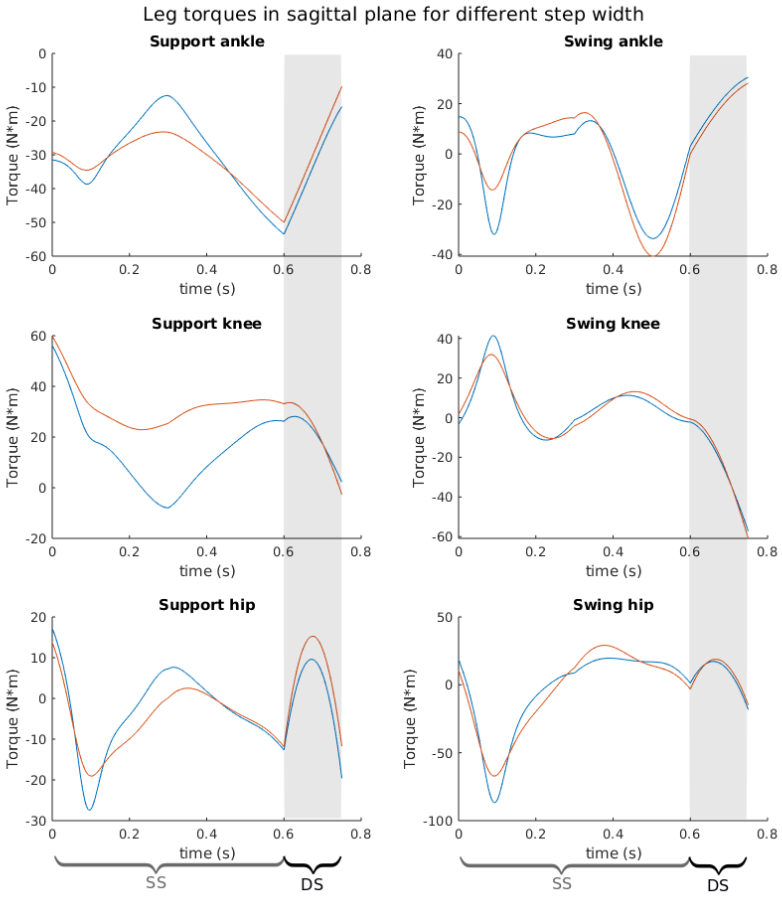

Fig. 15: The torque at the ankle, knee, and hip joints, in the sagittal plane for different periodic motions with a step length of 0.30m: step width 0.10m (blue) and 0.20m (red). A single step is represented. From time t = 0s to t=0.6s is the SS phase, from t=0.6s to 0.75s is the DS phase.

7.5 Effect of step length and width on the gait

The previous study was dedicated to the *Romeo* robot for which the choice of knee actuators does not allow a gait close to human walking, i.e. the evolution of the ZMP had to be adapted for this robot. If the study was dedicated to a more powerful robot, we could consider faster walks and greater variations in step length or width. Tests were carried out in simulation and the following properties were observed:

The step length does not have a great influence on the support leg torques, in the range 0.15 to 0.20m. For greater step lengths, such as 0.30m, we notice an increased torque in the support knee and hip, as well as in the swing leg, as illustrated on figure 14. The effect of the step width on the torques has also been investigated. In human gaits, the two factors that are most correlated to step width are the limb length and bi-acetabular breadth (width of the pelvis) [33, 34]. Human self-selected step width is around 0.15 $\times$ limb length, which is roughly equal to the bi-acetabular breadth. For Romeo, 0.15 $\times$ limb length is 0.10m, but pelvic width is much greater, at 0.192m. Therefore, we have tested step width values from 0.10 to 0.20m. We observed (see figure 15) that the hip torque decreased and knee torque mid-SS increased for increased step width. Eventually, we selected a 0.20m step width because of hip torque constraints.

We have also investigated the effect of the arm swing motion and observed that removing the arm swing reduced the torso torque.

8 Conclusion

The main characteristics of human walking are recalled to design a bio-inspired walking for the humanoid *Romeo*. However, the technological limits of *Romeo* are tacking into account in order to perform a feasible walking. The complete walking with a starting motion and a stopping motion is defined thanks to a strategy based on the *Essential model*. The specific definition the *essential model* allows to satisfy the constraint of the ZMP to be inside the convex hull of the support surface. The evolution of the 29 controlled variables which are the motions of the swing foot, the orientation of the upper bodies such as the trunk and the arms, allow to offer a visually pleasing movement of the humanoid robot by its similarities with the one of humans. The horizontal displacement of the CoM is not imposed and depends on the resulting dynamic of the bodies, the gravity effects, and the ZMP. For the walking trajectory defined for Romeo we investigated the effects of the choice of the ZMP trajectory to obtain the required joint torques. A correlation between the pose of the ZMP in sagittal plane and torque at ankle and knee in sagittal plane has been shown. The perspectives and future works are to test this complete walking motion experimentally.

References

1. M. Mori, "The uncanny valey," IEEE Robotics & Automation Magazine, vol. (Translated by Karl F. MacDorman and Norri Kageki), pp. 98–100, 2012.
2. D. Tlalolini, Y. Aoustin, and C. Chevallereau, "Design of a walking cyclic gait with single support phases and impacts for the locomotor system of a thirteen-link 3d biped using the parametric optimization," Multibody System Dynamics, vol. 23, no. 1, pp. 33–56, 2010.
3. A. D. Ames, "Human-inspired control of bipedal walking robots," IEEE Transactions on Automatic Control, vol. 59, no. 5, pp. 1115–1130, 2014.
4. S. Kajita, H. Hirukawa, K. Harada, and K. Yokoi, Introduction to humanoid robotics. Springer, 2014, vol. 101.
5. H. Razavi, A. M. Bloch, C. Chevallereau, and J. W. Grizzle, "Symmetry in legged locomotion: a new method for designing stable periodic gaits," Autonomous Robots, pp. 1–24, 2016.
6. T. Koolen, T. de Boer, J. Rebula, A. Goswami, and J. Pratt, "Capturability-based analysis and control of legged locomotion, part 1: Theory and application to three simple gait models," Int. J. of Robotics Research, vol. 31, no. 09, pp. 1094–1113, 2012.
7. K. Harada, K. Miura, M. Morisawa, K. Kaneko, S. Nakaoka, F. Kanehiro, T. Tsuji, and S. Kajita, "Toward human-like walking pattern generator," in IROS2009, St. Louis, USA, 2009, pp. 1071–1077.
8. C. Hayot, S. Sakka, V. Fohanno, and P. Lacouture, "Biomechanical modeling of the 3d center of mass trajectory during walking," Movement & Sport Sciences – Science & Motricité, no. 90, pp. 99–109, 2015, dOI: 10.1051/sm/2013047.
9. C. Chevallereau, H. Razavi, D. Six, Y. Aoustin, and J. Grizzle, "Self-synchronization and self-stabilization of 3d bipedal walking gaits," Robotics and Autonomous Systems, soumis.
10. S. H. Collins, P. G. Adamczyk, and A. D. Kuo, "Dynamic arm swinging in human walking," Proceeding of the Royal Society B: Biological Sciences, vol. 276, no. 1673, pp. 3679–3688, doi:10.1098/rspb.2009.0664, 2009.
11. Y. Aoustin and A. M. Formalskii, "3d walking biped: optimal swing swing of the arms," Multibody System Dynamics, pp. 55–66, 2014.
12. S. Sakka, L. P. Poubel, and D. Cehajic, "Tasks prioritization for whole-body realtime imitation of human motion by humanoid robots," in Digital Intelligence (DI2014), 2014, pp. 5–p.
13. J. B. Cole, D. B. Grimes, and R. P. N. Rao, "Learning full-body motions from monocular vision: dynamic imitation in a humanoid robot," in 2007 IEEE/RSJ International Conference on Intelligent Robots and Systems, 2007, pp. 240–246.
14. K.-S. Hwang, W.-C. Jiang, Y.-J. Chen, and H. Shi, "Motion segmentation and balancing for a biped robot's imitation learning," IEEE Transactions on Industrial Informatics, vol. 13, no. 3, pp. 1099–1108, 2017.
15. V. De-León-Gómez, Q. Luo, A. Kalouguine, J. A. Pámanes, Y. Aoustin, and C. Chevallereau, "An essential model for generating walking motions for humanoid robots," Robotics and Autonomous Systems, vol. 112, pp. 229–243, 2019.
16. M. Anderle and S. Celikovskỳ, "Cyclic walking-like trajectory design and tracking in mechanical chain with impacts," in Proc. of the XXIth Congreso ACCA, 2014, pp. 341–346.
17. J. Rose and J. G. Gamble, Human walking, 3rd ed. Williams & Wilkins, 2006.
18. M. S. Orendurff, A. D. Segal, G. K. Klute, J. S. Berge, E. S. Rohr, and N. J. Kadel, "The uncanny valley." Journal of Rehabilitation Research & Development, vol. 41, no. 6, 2004.
19. T. Jurcevic Lulic and O. Muftic, "Trajectory of the human body mass centre during walking at different speed," in DS 30: Proc. of DESIGN 2002, the 7th Int. Design Conf., Dubrovnik, 2002.
20. M. Grundy, P. Tosh, R. McLeish, and L. Smidt, "An investigation of the centres of pressure under the foot while walking," J. of bone and joint surgery. British volume, vol. 57, no. 1, pp. 98–103, 1975.
21. P. Sardain and G. Bessonnet, "Zero moment point-measurements from a human walker wearing robot feet as shoes," IEEE Trans. on Systems, Man, and Cybernetics-Part A: Systems and Humans, vol. 34, no. 5, pp. 638–648, 2004.
22. A. Thorstensson, J. Nilsson, H. Carlson, and M. R. ZOMLEFER, "Trunk movements in human locomotion," Acta Physiologica Scandinavica, vol. 121, no. 1, pp. 9–22, 1984.
23. P. Meyns, S. M. Bruijn, and J. Duysens, "The how and why of arm swing during human walking," Gait & posture, vol. 38, no. 4, pp. 555–562, 2013.

24. Y. Aoustin and A. M. Formalskii, "3d walking biped: optimal swing of the arms," Multibody System Dynamics, vol. 32, no. 1, DOI 10.1007/s11044-013-9378-3, pp. 55–66, 2014.
25. C. C. Kemp, P. Fitzpatrick, H. Hirukawa, K. Yokoi, K. Harada, and Y. Matsumoto, "Humanoids," in Springer handbook of robotics. Springer, 2008, pp. 1307–1333.
26. D. A. Winter, "Foot trajectory in human gait: a precise and multifactorial motor control task," Physical therapy, vol. 72, no. 1, pp. 45–53, 1992.
27. T. Kinugasa, C. Chevallereau, and Y. Aoustin, "Effect of circular arc feet on a control law for a biped," Robotica, vol. 27, no. 4, pp. 621–632, 2008.
28. D. E. Orin, A. Goswami, and S.-H. Lee, "Centroidal dynamics of a humanoid robot," Autonomous Robots, vol. 35, no. 2-3, pp. 161–176, 2013.
29. J. Carpentier and N. Mansard, "Multicontact locomotion of legged robots," IEEE Transactions on Robotics, vol. 34, no. 6, pp. 1441–1460, 2018.
30. M. Vukobratovic and B. Borovac, "Zero-moment point-thirty five years of its life," Int. J. of Humanoid Robotics, vol. 1, no. 1, pp. 157–173, 2004.
31. Y. Jian, D. A. Winter, M. G. Ishac, and L. Gilchrist, "Trajectory of the body cog and cop during initiation and termination of gait," Gait & Posture, vol. 1, no. 1, pp. 9–22, 1993.
32. H. Pontzer, J. H. Holloway, D. A. Raichlen, and D. E. Lieberman, "Control and function of arm swing in human walking and running," The Journal of Experimental Biology, vol. 212, pp. 523–534, 2009.
33. L. T. Gruss, R. Gruss, and D. Schmitt, "Pelvic breadth and locomotor kinematics in human evolution," The Anatomical Record, vol. 300, no. 4, pp. 739–751, 2017.
34. J. Maxwell Donelan, R. Kram, and K. Arthur D, "Mechanical and metabolic determinants of the preferred step width in human walking," Proceedings of the Royal Society of London. Series B: Biological Sciences, vol. 268, no. 1480, pp. 1985–1992, 2001.